Quantum carpets woven by Wigner functions

2000 New J. Phys. 2 4

(http://iopscience.iop.org/1367-2630/2/1/004)

New Journal of Physics
An Institute of Physics and Deutsche Physikalische Gesellschaft Journal

Quantum carpets woven by Wigner functions

O M Friesch†, I Marzoli‡ and W P Schleich†

† Abteilung für Quantenphysik, Universität Ulm, 89069 Ulm, Germany
‡ Dipartimento di Matematica e Fisica and INFM, Università di Camerino, 62032 Camerino, Italy
E-mail: marzoli@campus.unicam.it

New Journal of Physics **2** (2000) 4.1–4.11 (http://www.njp.org/)
Received 13 October 1999; online 6 March 2000

Abstract. The dynamics of many different quantum systems is characterized by a regular net of minima and maxima of probability stretching out in a spacetime representation. We offer an explanation to this phenomenon in terms of the Wigner function. This approach illustrates very clearly the crucial role played by interference.

1. Introduction

The representation of the probability distribution of one-dimensional quantum systems, as a function of position and time, often displays unexpected regularities in the long time evolution. Besides the full and fractional revivals [1]–[5] taking place at well defined times, the complete spacetime picture is characterized by highly ordered patterns of minima (canals) and maxima (ridges) of probability.

In figures 1, 2 and 3 we show such structures for wave packets propagating in an infinitely deep potential well, a harmonic oscillator potential and a quartic potential. For obvious reasons, the name *quantum carpet* has emerged to describe this phenomenon. Quantum carpets appear in many fields of wave physics ranging from quantum mechanics, with applications in nuclear physics [6] and Bose–Einstein condensation [7], to electromagnetic waves and, in particular, waveguides.

Various explanations of this phenomenon have been offered [5], [8]–[18]. In this paper, however, we use the unique advantages of an electronic journal to visualize an approach [11, 12] based on the Wigner function [19]. We present a collection of movies illustrating very clearly how the Wigner function weaves quantum carpets. For simplicity, we restrict ourselves to the problem of a particle in a box, even though our conclusions apply equally well to a much more general class of systems.

The paper is organized as follows: in order to introduce the reader to this phenomenon, we present a collection of quantum carpets for various potentials in section 2. In section 3, we then show in a movie how these structures make their appearance in the dynamics of the wave packet.

1367-2630/00/000004+11$30.00

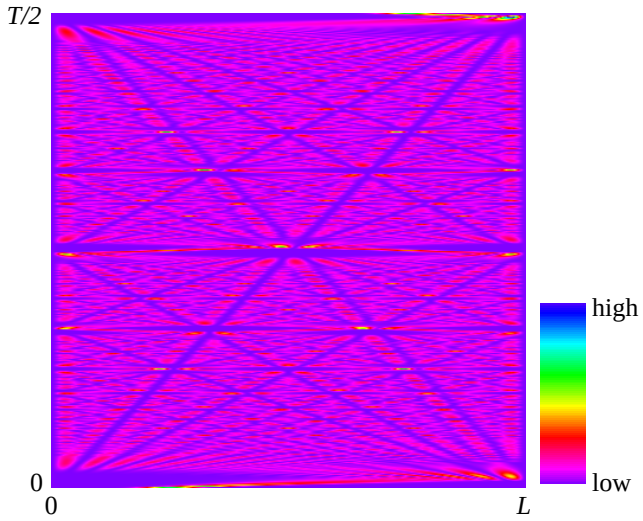

Figure 1. Density plot of the probability density $|\psi(x,t)|^2$ to find the particle at position x at time t for an initial Gaussian wave packet centred on $\bar{x} = L/4$, having width $\sigma = L/20$ and average momentum $\bar{p} = 15\hbar\pi/L$. The height of the plot is represented by the colours shown in the bar on the right-hand side.

Here, and in the remainder of the paper, we confine ourselves to the problem of the particle in a box. In section 4 we use a representation of the probability density in terms of Wigner functions derived in references [11, 15] to identify the interference terms, that is, the *ghost* terms. These are responsible for the pattern formation. Our concluding remarks are given in section 5.

2. A collection of quantum carpets

The first striking example of a quantum carpet emerged from numerical simulations performed on a particle confined to an infinitely deep potential well [20].

As shown in figure 1, the initial Gaussian probability distribution of finding the particle at position x at time t gives rise to a rich pattern of straight world lines of the form

$$\frac{t}{T/2} = \frac{1}{q}\frac{x}{L} + \text{constant} \tag{1}$$

with q being always an integer number. Here T is the revival time and L denotes the width of the box. In figure 1, we can easily distinguish the lines corresponding to $q = \pm 1, \pm 2, \pm 3, \ldots$.

Note that canals and ridges of probability depart from the corners or enter from the sides, while the particle started from $x = L/4$. Moreover, these structures correspond to very small momenta, which have an exponentially small weight in the original wave packet centred at a large average momentum. Further studies [8, 9] have proved that the overall features of the spacetime structures, like the position and the steepness of the world lines, are independent of the initial conditions.

A general explanation for this phenomenon rests on multimode interference [13]. The initial wave packet encompasses many excited modes of the system, which interfere pairwise; each pair of modes produces a so-called *intermode trace* in the probability distribution. These traces correspond to lines of constant phase in spacetime and their visibility is enhanced by degeneracy

[13, 15, 16]. The most pronounced structures are due to the superposition of many intermode traces, created by pairs of different eigenmodes. Here the spectrum of energies enters in a crucial way: one finds the highest degeneracy in strongly confining potentials, whose best example is provided by the infinitely deep square well, while the opposite extreme case of very poor overlap among intermode traces is represented by the harmonic oscillator.

Indeed, in the case of the harmonic oscillator, the linear dependence of the energy levels on the quantum number n reduces the degeneracy and washes out the patterns. A possible way to restore them is a careful choice of the initial wave packet. When we consider a wave packet made up only of energy eigenstates with quantum numbers being perfect squares, such as n = 0, 1, 4, 9,. . ., the initial condition introduces the required degeneracy among the intermode traces.

Figure 2 shows the resulting structures in the probability distribution. These patterns appear predominantly near the bottom of the potential, where the particle behaves almost like a free particle. Here, a rich pattern of canals and ridges develops, similar to the case of a particle in a box.

However, it is not always necessary to engineer the appropriate initial wave packet in order to observe ordered structures in the probability distribution. As mentioned before, hard wall potentials are good candidates for producing quantum carpets. One should, therefore, expect to see patterns for an anharmonic potential $U(x) \propto x^4$ [14], which is an intermediate case between the infinite square well and the harmonic oscillator. In figure 3 we display the time evolution of the probability distribution starting with the ground state wave function hit by a short pulse delivering an average momentum $\bar{p}$. Enough states are populated in order to produce intermode traces that are almost straight lines. Indeed, the shape of the structures depends on the specific potential under consideration; strictly speaking, straight lines are another special feature of the box, while, in general, curved lines are to be expected.

We conclude this section by mentioning that the formalism of intermode traces [13, 14] applies to any kind of potential. We can, therefore, identify the pairs of eigenmodes generating each trace and classify them into two categories: quantum traces and classical ones. The latter ones are reminiscent of the classical motion of the particle, which is still visible before the wave packet collapses, as shown in the first couple of cycles in figure 3.

3. Order in the dynamics of the wave packet

The problem of a particle confined to an infinitely deep square well is the most elementary problem in quantum mechanics. For this example the probability amplitude $\psi(x,t)$ to find the particle of mass M at time t at the position x in the box of length L reads

$$\psi(x,t) = \sum_{m=1}^{\infty} \psi_m \sin\left(m\pi\frac{x}{L}\right) \exp\left(-2\pi \mathrm{i} m^2 \frac{t}{T}\right). \tag{2}$$

Here the quantities ψ_m are the expansion coefficients of the initial wave packet $\psi(x, t = 0) \equiv \varphi(x)$ into the energy wave functions [21]

$$u_m(x) = \sqrt{\frac{2}{L}} \sin(k_m x) \tag{3}$$

with wave numbers

$$k_m \equiv m\frac{\pi}{L} \tag{4}$$

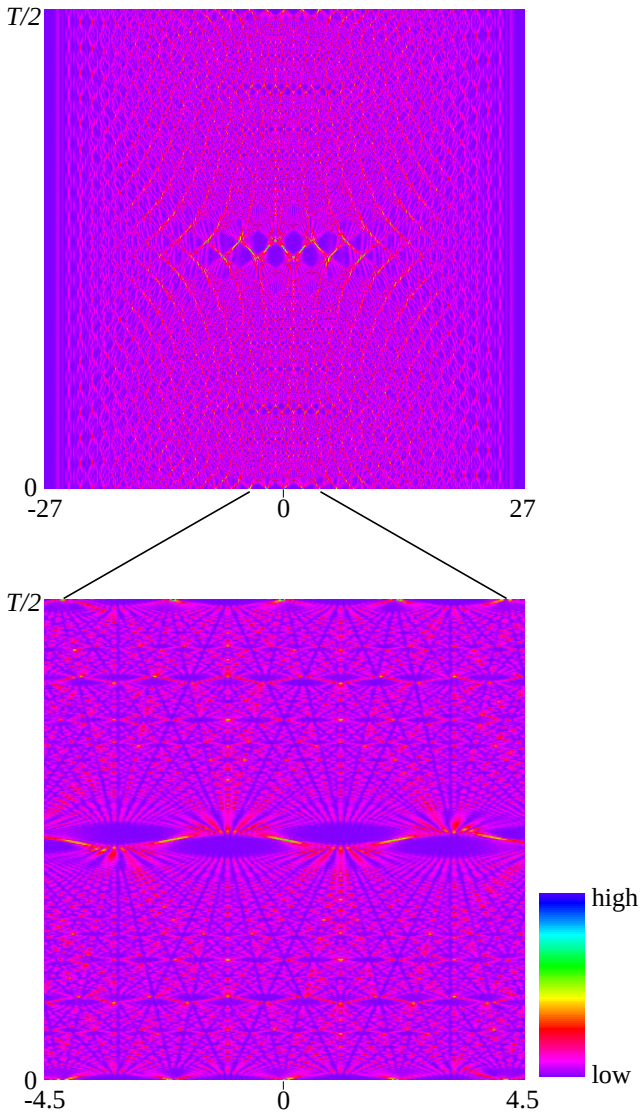

Figure 2. Top: density plot of the probability density $|\psi(x,t)|^2$ for a specially tailored wave packet moving in a harmonic potential. Only eigenstates with quadratic quantum numbers, n = 0, 1, 4, 9,. . ., enter into play. Bottom: we show a magnified view around the centre of the potential. Lengths are expressed in units of $\sqrt{\hbar/M\omega}$, with M being the mass of the particle and ω the frequency of the harmonic oscillator. Here $T \equiv 2\pi/\omega$ is the oscillation period. In both pictures we use the colour coding shown in the bar on the right-hand side.

and eigenenergies

$$E_m \equiv \frac{(\hbar k_m)^2}{2M} = m^2 \hbar \frac{2\pi}{T}. \tag{5}$$

In the last expression, as well as in equation (2), we have introduced the revival time

$$T \equiv \frac{4ML^2}{\hbar\pi} \tag{6}$$

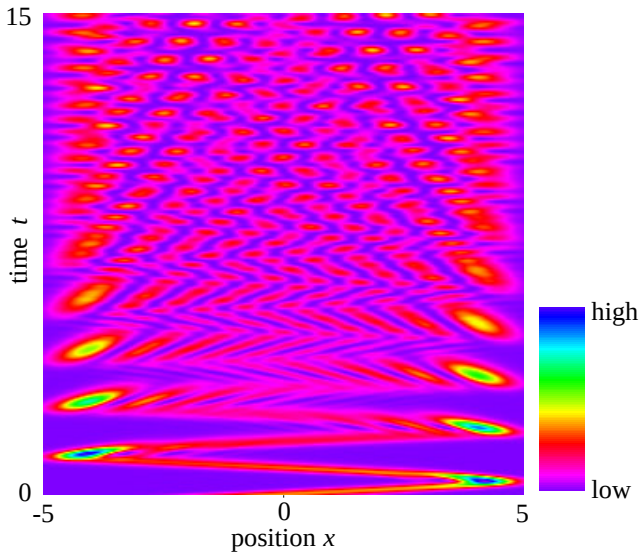

Figure 3. Density plot of the probability density $|\psi(x,t)|^2$ for the ground state function moving with average momentum $\bar{p}$ in the anharmonic potential $U(x) = Ax^4$. Lengths and time are scaled, respectively, by the factors $x_s \equiv (\hbar^2/MA)^{1/6}$ and $t_s \equiv (M^2/\hbar A)^{1/3}$. The colour coding is shown in the bar on the right-hand side.

at which the wave function is identical to its initial form at $t = 0$, that is

$$\psi(x, t = T) = \psi(x, t = 0). \tag{7}$$

In the first video sequence we present the resulting time evolution of the probability distribution $|\psi(x,t)|^2$. The initial wave function is a Gaussian wave packet, centred around $x = L/4$, with width $\sigma = L/20$ and average momentum $\bar{p} = 15\hbar\pi/L$.

To guide the reader's eyes, we have put two arrows underneath the position axis. These arrows move with constant velocity and bring out in this way the underlying regularity in the wave packet dynamics, which otherwise would not be apparent because of fast oscillations. The left-hand arrow is always pointing to a minimum in the probability density, while the right-hand one is sometimes at a maximum and sometimes at a minimum. In the spacetime density plot of figure 1, the arrows move along the two main diagonals: one arrow, connecting the left-hand lower corner with the right-hand upper one, is a canal between two ridges and the other one, connecting the lower right-hand corner with the left-hand upper one, is a chopped ridge between two canals.

In the video sequence, the rectangular bar on the left-hand side indicates time. On this 'time thermometer' we have marked important fractions of the revival time T. The revival time is the natural time scale of the problem since, according to equation (7), the probability amplitude is identical to that at time $t = 0$. However, at $T/2$ the wave packet has already reshaped itself, even though it takes a different phase and the probability density happens to be the mirror image of the initial one. Moreover, for the sake of brevity, we only follow the wave packet dynamics until $T/4$, which is, nevertheless, a sufficiently long time interval to appreciate the essential features of the system evolution.

At fractions of the revival time T, the probability density splits up into several replicas of the initial Gaussian distribution. Here we do not enter the theory of the fractional revivals [1]–[5], but want to draw attention to the most remarkable snapshots: for example, we note three wave packets appearing at $t = T/6$ or two counterpropagating ones at $t = T/4$. For a detailed discussion of the behaviour of the wave function at and in the neighbourhood of a fractional revival, we refer the reader to reference [22].

4. Wigner function approach

In this section we analyse the mechanism responsible for the appearance of spacetime structures in the probability density. To this end we adopt an approach based on the Wigner function. For the sake of brevity, we do not present the complete derivation here, but rather visualize the essential results in an innovative and effective way, that is, by means of video sequences.

From expression (2) for the probability amplitude, it is not obvious how the patterns of the carpets emerge. To bring this out more clearly we recall an expression for the probability density as a sum over Wigner functions, derived in references [11, 15]. This representation reads

$$|\psi(x,t)|^2 = \frac{\pi\hbar}{2L} \sum_{n,l=-\infty}^{+\infty} (-1)^{nl} W_\phi[\xi_{n,l}(x,t), p_n] \tag{8}$$

where

$$W_\phi(x,p) \equiv \frac{1}{2\pi\hbar} \int_{-\infty}^{+\infty} \mathrm{d}y\, \mathrm{e}^{\mathrm{i}py/\hbar} \phi\left(x - \frac{y}{2}\right) \phi^*\left(x + \frac{y}{2}\right) \tag{9}$$

is the Wigner function of the antisymmetric wave function

$$\phi(x) \equiv \varphi(x) - \varphi(-x) \tag{10}$$

built out of the original wave packet $\varphi(x)$ and its mirror image. (Note that there are at least two ways to derive expression (8). The first approach [15] relies on the standard representation (2) of the wave function, calculates the absolute value squared, and rewrites the resulting double sum using a generalized Poisson summation formula [15]. The second approach [11] uses the concept of the Wigner function and, following an idea of Max Born [23], replaces the propagation of the single wave packet in a box by the free propagation of an array of antisymmetric wave packets.)

Moreover, we have introduced the world lines

$$\xi_{n,l}(x,t) \equiv x - n\frac{L}{T/2}t - lL \tag{11}$$

and the momenta

$$p_n \equiv np_1 \equiv n\frac{\pi\hbar}{2L}. \tag{12}$$

We point out that the world lines of equation (11) for $\xi_{n,l} \equiv 0$ reduce to the form of equation (1), which describes the shape of the canals and ridges giving rise to the quantum carpet. Hence, the probability density consists of a superposition of Wigner functions aligned along straight lines, defined by $\xi_{n,l}(x,t)$. This is the first clue of the appearance of spacetime structures in the probability density of a particle confined to an infinitely deep potential well.

According to equation (2) the wave function displays a periodicity in space with period $2L$. This manifests itself in a quantization (equation (12)), of the momentum. In the representation of equation (8), the summation over n accounts for this quantization of momentum. The other

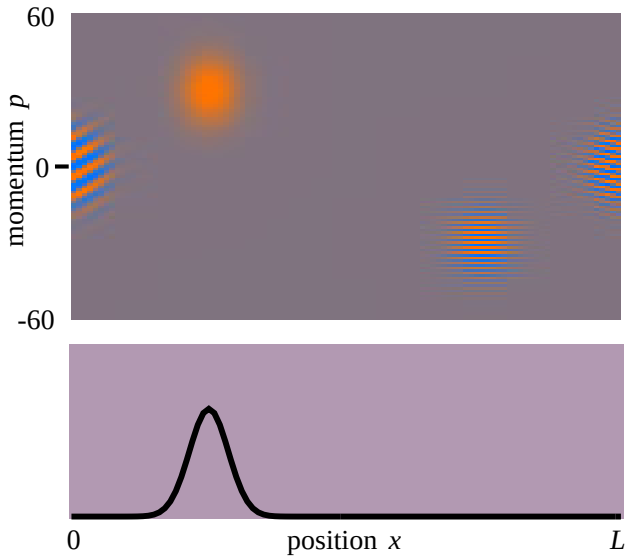

Figure 4. Top: Wigner function in phase space for the periodic array of antisymmetric wave functions. We restrict the picture to the physically relevant portion of the position axis, namely the box width. Momentum is expressed in units of $p_1 \equiv \hbar\pi/2L$. Orange areas correspond to positive parts of the Wigner function, while blue shows the negative parts. Bottom: the resulting probability distribution to find the particle at position x at time $t = 0$.

summation index l labels the walls of the original box and of its infinitely many replicas resulting from the $2L$ periodicity of the energy wave functions.

From equations (8) and (11) we note that the time evolution of the probability density follows from the time evolution of the Wigner function of the antisymmetric superposition state ϕ. This time evolution is very simple: the position variable x is replaced by $x - (p_n/M)t$. Therefore, in order to understand the time evolution of the probability density we have to consider the free evolution of the array

$$W_\psi(x, p_n) = \frac{\pi\hbar}{2L} \sum_{n,l=-\infty}^{+\infty} \delta(p - p_n)(-1)^{nl} W_\phi(x - lL, p_n) \tag{13}$$

of Wigner functions.

We now take advantage of the multimedia capabilities of the journal to show the time evolution of the Wigner function (second video sequence) and the resulting quantum carpet. This animation displays the Wigner function in the upper diagram, and the corresponding probability distribution in the lower one.

We can find the probability density geometrically by integrating the Wigner function over momentum. To familiarize the reader with this presentation, we display in figure 4 the Wigner function at time $t = 0$ (top) and the resulting probability distribution inside the box (bottom). We restrict the view of (x, p) phase space to the elementary box between $[0,L]$ and do not show the images lying outside. In our colour coding, blue tones are assigned to negative values, and orange to positive ones. The vertical axis of the (x, p) phase space is centred around zero momentum.

Beside the orange ellipse, located in $x = L/4$ and $p = \bar{p}$, which corresponds to the Wigner

function $W_\varphi(x,p)$ of the original Gaussian wave packet, there are three *ghost* terms. These terms, which initially do not contribute to the probability distribution because of their oscillatory behaviour, play a fundamental role in weaving the quantum carpets. They result from the bilinearity of the Wigner function (equation (9)), in the wave function. Indeed, the Wigner function of the superposition $\phi(x)$ (equation (10)), reads

$$W_\phi(x,p) = W_\varphi(x,p) + W_\varphi(-x,-p) + W_{\rm int}(x,p). \tag{14}$$

Here $W_\varphi(x,p)$ and $W_\varphi(-x,-p)$ correspond to the two wave packets $\varphi(x)$ and $\varphi(-x)$ building up $\phi(x)$ and

$$W_{\rm int}(x,p) \equiv -\frac{1}{2\pi\hbar}\int_{-\infty}^{+\infty} {\rm d}y\, {\rm e}^{{\rm i}py/\hbar}\varphi\left(x-\frac{y}{2}\right)\varphi^*\left(-x-\frac{y}{2}\right) + {\rm c.c.} \tag{15}$$

is the *ghost* interference term. This term is responsible for the two ellipses located at the walls of the box and centred around $p = 0$. The location of these two ellipses explains why the quantum carpets consist of a net of straight lines departing always from the walls of the box, regardless of the actual position of the particle at time $t = 0$. Hence, the Wigner function $W_\varphi(x,p)$ associated with the original wave packet $\varphi(x)$ cannot be involved in the pattern formation. The third horizontally striped ellipse represents, instead, an interference term due to the $2L$ periodicity.

We now turn to the time evolution (second video sequence) of the initial distribution presented in figure 4. Components with a positive momentum move to the right, while those with a negative momentum propagate to the left. Moreover, each momentum component proceeds at a different speed, leading to a shearing of the initially slightly elliptical shape of the Wigner function. Reflections at the walls are automatically taken into account by our periodic representation: terms leaving the box re-enter the scene from the same side, but with reversed momentum.

After the early stage of the dynamics, during which the wave function spreads and starts to interfere with itself, giving rise to the oscillations in the probability distribution, an almost complete collapse occurs. At the same time positive, negative and oscillatory terms of the Wigner function are completely mixed up. However, at fractions of the revival time they rearrange in an ordered way to produce the fractional revivals and eventually, at $t = T/2$, they create the full revival.

To gain more insight into the spacetime structures, we now concentrate on the central part of the Wigner function, around momentum $p = 0$. The third video sequence shows in the upper diagram a magnified view of the Wigner function, with the momentum ranging from $-3p_1$ to $3p_1$. These components belong to the interference terms $W_{\rm int}(x,p)$ produced by the antisymmetric superposition. In the lower diagram, we show the spacetime representation of the probability density evolving with time. This diagram starts from an essentially empty picture and slowly builds up the carpet.

Canals and ridges depart from both corners. This is due to the fact that the interference terms of the Wigner function are initially aligned at $x = 0$ and $x = L$. Due to the different momenta they separate from each other, carving canals and mounting ridges along straight lines of fixed steepness. The slope of the spacetime structures is governed by the quantized momenta p_n. As one can see from expression (11) for the world lines, smaller momenta correspond to straight lines with larger steepness. These are also the most pronounced structures of the pattern and, for this reason, we focus on the terms in the Wigner function around $p = 0$.

In order to follow in more detail the dynamics of the Wigner function and the corresponding progressive weaving of the quantum carpet, we first highlight two terms of the Wigner function

and the related world lines in the probability distribution. These are the momenta $p = \pm p_1$ associated with the main diagonals of the carpet. Here we have marked with the same colour the components of the Wigner function and the corresponding structures in the carpet. We clearly recognize that the oscillations in the interference terms manifest themselves in the canals and ridges along the corresponding world line.

We now turn to the components of the Wigner function with momenta $p = \pm 2p_1$, which are responsible for the canals and ridges reaching the sides at $T/4$ (fourth video sequence). The zig-zag pattern is due to the fact that at $T/4$ the terms in the Wigner function undergo a reflection at the walls, i.e. they leave the box and immediately re-enter with reversed momentum, thus producing structures with opposite slopes. This explains why canals and ridges always arise either from the corners or from the sides of the spacetime picture. All the world lines converge eventually, at $t = T/2$, while the interference terms of the Wigner function realign themselves at the box walls.

5. Conclusions

The quantum carpet woven by a particle confined to an infinitely deep square well can be described by the time evolution of a periodic array of Wigner functions undergoing free evolution. The interference terms of the Wigner function manifest themselves in the highly regular spacetime structures in the probability distribution. Indeed, the results of our videos provide clear evidence of the one-to-one correspondence between the interference components, around $p = 0$, of the Wigner function and the world lines in the probability density. We can, therefore, conclude that the Wigner function is a useful tool for investigation of the origin of the quantum carpets and, in particular, to illustrate the role of interference.

Acknowledgments

We express our gratitude to P J Bardroff, M V Berry, I Bialynicki-Birula, J H Eberly, M Fontenelle, F Großmann, M Hall, A E Kaplan, H J Kimble, T Kiss, W E Lamb Jr, K A H van Leeuwen, C Leichtle, J Marklof, M M Nieto, J M Rost, P Stifter and E C G Sudarshan for many fruitful discussions on this topic. One of us (IM) acknowledges the kind hospitality and support during her visit at the Universität Ulm and especially the TMR Research Network *Microlasers and Cavity QED*. The work by WPS was also supported by DFG.

References

[1] Parker J and Stroud C R Jr 1986 *Phys. Rev. Lett.* **56** 716
[2] Averbukh I Sh and Perelman N F 1989 *Phys. Lett.* A **139** 449
Averbukh I Sh and Perelman N F 1989 *Sov. Phys. JETP* **69** 464
[3] Leichtle C, Averbukh I Sh and Schleich W P 1996 *Phys. Rev. Lett.* **77** 3999
Leichtle C, Averbukh I Sh and Schleich W P 1996 *Phys. Rev.* A **54** 5299
[4] Aronstein D L and Stroud C R Jr 1997 *Phys. Rev.* A **55** 4526
[5] A similar phenomenon in the context of optics is the Talbot effect. See, for example,
Berry M V and Klein S 1996 *J. Mod. Optics* **43** 2139
[6] Rozmej P and Arvieu R 1998 *Phys. Rev.* A **58** 4314
[7] Wright E M, Wong T, Collett M J, Tang S M and Walls D F 1997 *Phys. Rev.* A **56** 591

[8] Berry M V 1996 *J. Phys. A: Math. Gen.* **29** 6617
[9] Großmann F, Rost J-M and Schleich W P 1997 *J. Phys. A: Math. Gen.* **30** L277
[10] Marklof J 1997 *Limit Theorems for Theta Sums with Applications in Quantum Mechanics* (Aachen: Shaker)
[11] Stifter P, Leichtle C, Schleich W P and Marklof J 1997 *Z. Naturforsch. a* **52** 377
[12] I. Marzoli, Friesch O M and Schleich W P 1998 *Proc. Fifth Wigner Symposium* ed P Kasperkovitz and D Grau (Singapore: World Scientific)
[13] Kaplan A E, Stifter P, van Leeuwen K A H, Lamb W E Jr and Schleich W P 1998 *Physica Scripta* T **76** 93
[14] Kaplan A E, Marzoli I, Lamb W E Jr and Schleich W P 2000 *Phys. Rev.* A **61** 032101
[15] Marzoli I, Saif F, Bialynicki-Birula I, Friesch O M, Kaplan A E and Schleich W P 1998 *Acta Physica Slovaca* **48** 323
[16] Marzoli I, Bialynicki-Birula I, Friesch O M, Kaplan A E and Schleich W P 1999 *Nonlinear Dynamics and Computational Physics* ed V B Sheorey (New Delhi: Narosa). See also the Los Alamos e-Print archive: quant-ph/9804015 (1998)
[17] Berry M V and Bodenschatz E 1999 *J. Mod. Optics* **46** 349
[18] Hall M J W, Reineker M S and Schleich W P 1999 *J. Phys. A: Math. Gen.* **32** 8275
[19] Hillery M, O'Connell R F, Scully M O and Wigner E P 1984 *Phys. Rep.* **106** 121
[20] Kinzel W 1995 *Phys. Bl.* **51** 1190
[21] See, e.g. Bohm D 1951 *Quantum Theory* (Englewood Cliffs, NJ: Prentice Hall)
[22] Stifter P, Lamb W E Jr and Schleich W P 1997 *Proc. Conf. Quantum Optics and Laser Physics* ed L Jin and Y S Zhu (Singapore: World Scientific)
[23] Born M and Ludwig W 1958 *Z. Phys.* **150** 106

Video sequences

Video sequence 1

In this movie we present the time evolution of the probability density $|\psi(x,t)|^2$ to find the particle at time t at position x in a box of width L. The initial wave function is a Gaussian wave packet, centred around $\bar{x} = L/4$, having width $\sigma = L/20$ and an average momentum $\bar{p} = 15\hbar\pi/L$. To illustrate the regularity in the wave packet dynamics, we have placed two arrows, moving with constant velocity, underneath the position axis. The left-hand arrow always points to a minimum in the probability density (canal), while the right-hand arrow is sometimes at a minimum and sometimes at a maximum (chopped ridge). The rectangular bar on the left-hand side indicates time. We have marked on it important fractions of the revival time T, at which we can observe the fractional revivals of the wave packet. Especially remarkable are the revivals occurring at $T/6$ and $T/4$, characterized, respectively, by the appearance of three and two replicas of the original wave packet.

Video sequence 2

The upper part of this animation shows the time evolution of the Wigner function, and the lower one shows the resulting probability distribution of finding the particle in the box. The Wigner function is plotted in phase space, where the horizontal axis corresponds to position and the vertical axis, on which we have marked the zero, corresponds to momentum. Positive values are displayed in orange, and negative ones are shown in blue. The movie starts from the situation depicted in figure 4 and follows the dynamics up to $t = T/2$, when the wave packet reshapes itself. Also, the time evolution of the Wigner function is characterized by fractional revivals culminating in the full revival at $T/2$.

Video sequence 3

We concentrate on the enlarged view of the central part of the Wigner function, around momentum $p = 0$. This magnified portion encompasses interference terms with momentum ranging from $-3p_1$ to $3p_1$. In the lower diagram, we follow the simultaneous weaving of the quantum carpet. To make clear the correspondence between the interference terms of the Wigner function and the world lines in the probability distribution, we mark, with the same colour, the components of the Wigner function with momenta $\pm p_1$ and the corresponding structures in the carpet.

Video sequence 4

We show the same sequence as in the previous animation, but this time we highlight the terms in the Wigner function with momenta $\pm 2p_1$ and the corresponding zig-zag patterns in the quantum carpet.